Nuclear Inst. and Methods in Physics Research, A 1048 (2023) 167918

Contents lists available at ScienceDirect

Nuclear Inst. and Methods in Physics Research, A

journal homepage: www.elsevier.com/locate/nima

Europium doped Gd_2O_3 and $GdBO_3$ scintillators for thermal neutron detection

G.M. Nadeera Hemamali [a,*], D.R. Smith [a], P.R. Hobson [a,b], G. Fern [a], T. Ireland [a]

[a] Department of Electronic and Electrical Engineering, Brunel University London, United Kingdom
[b] Department of Physics and Astronomy, Queen Mary University of London, United Kingdom

ARTICLE INFO

Dataset link: http://10.6084/m9.figshare.20521023

Keywords:
Neutron detection
Gadolinium
Scintillator
An alternative to ^{3}He

ABSTRACT

Neutron detectors used in various applications in nuclear security and nuclear safety are mostly based on the ^{3}He technology. Unfortunately, in the last few years, the market of ^{3}He has encountered huge problems in matching the supply and demand leading to an exponential increase in the price and a serious strategic problem of resources. To guarantee the availability of detection systems for nuclear security, the last decade has been driven by the quest for exploring alternative technologies to replace ^{3}He based detectors. Gadolinium (^{nat}Gd) is a promising rare earth element which has the largest capture cross-section for thermal neutrons among all stable elements due to the contributions of the isotopes ^{155}Gd and ^{157}Gd. This paper describes the fabrication of Gd_2O_3:Eu^{3+} and $GdBO_3$:Eu^{3+} phosphors as scintillators for thermal neutron detection. The samples were evaluated using photoluminescence, SEM analysis, and pulse height spectra recorded from a D–D neutron source. The recorded spectrum was compared to a FLUKA simulation of the characteristic K X-ray emission following neutron capture.

1. Introduction

Neutron detectors are mainly used in nuclear security and nuclear safety to prevent and detect illicit transportation of special nuclear materials (SNMs). Detection of illicit trafficking of such materials relies on the radiation emitted since SNMs emit neutrons through spontaneous fission that can be detected at longer distances and are more difficult to shield. For this reason, neutron detectors offer an important role in detection systems. Existing neutron detection systems are typically based on the ^{3}He technology. Its high neutron detection efficiency, nearly perfect gamma-ray discrimination and non-toxicity make them ideal for nuclear security applications.

^{3}He based neutron detectors require pure ^{3}He, which is a rare non-radioactive isotope of helium. ^{3}He is only produced as a byproduct of tritium decay [1]. In recent years, because of the increasing demand for ^{3}He in instrumentation for nuclear security and in other science applications, the need for ^{3}He has grown significantly, while current stockpiles around the world have been decreasing since the year 2000. The growing demand for ^{3}He already exceeds planned production over the next few years which has led to dramatic increases in its price [2,3]. By contrast, the deflated price for gadolinium oxide has steadily fallen over the last two decades [4]. The last decade has been driven by the quest for finding competitive alternative technologies to replace ^{3}He based detectors, to guarantee the availability of detection systems for nuclear security applications. It will be very unlikely to develop neutron detectors having characteristics better than those based on ^{3}He. Therefore, a suitable alternative does not need to be necessarily better than ^{3}He but simply should fulfill the minimum requirements to detect the neutrons, which are derived from international standards [5–7] and are that the instrument shall indicate the presence of neutron radiation. If the instrument responds in count rate, no further testing is required.

Thus, intense research and development continue to explore new phosphor materials as scintillators or the optimization of the current ones taking advantage of new technological methods for their preparation. Therefore, the development of a phosphor with rare earth elements such as gadolinium shows a high potential for the deployment of efficient and cost-effective inorganic scintillators for neutron detection.

Gadolinium (^{nat}Gd) is a rare earth element that processes the largest thermal neutron absorption cross-section of all the stable elements, with a total neutron absorption cross-section of nearly 48,800 barns. The natural abundance of ^{155}Gd and ^{157}Gd isotopes in ^{nat}Gd are 14.8% and 15.6% respectively, contributing most significantly to the thermal neutron absorption cross-section, approximately 99.99% of the elemental cross-section [8].

There are no heavy ions emitted after a Gd atom captures a neutron, unlike the thermal neutron radiative capture in ^{3}He, ^{6}Li, and ^{10}B, where heavily charged particles with distinguished energies are emitted

* Corresponding author.
E-mail address: eepgnng1@brunel.ac.uk (G.M. Nadeera Hemamali).

https://doi.org/10.1016/j.nima.2022.167918
Received 5 September 2022; Received in revised form 16 November 2022; Accepted 11 December 2022
Available online 19 December 2022

Table 1
Summary of photon emission of interest in this study [12,13].

Isotope	Abundance (%)	Emitted Photon	Energy (keV)	Emission probability (%)
^{157}Gd	15.6	ɤ-ray	181.9	18.33 ± 1.69
		ɤ-ray	79.5	9.75 ± 0.69
		K_α	43	18.2 ± 1.0
		K_β	49	4.5 ± 0.3
^{155}Gd	14.8	K_α	43	29.1 ± 3.8
		K_β	49	7.1 ± 0.9

in producing subsequent signals in the detector. For example, as shown in Eq. (1), the de-excitation of ^{157}Gd following the absorption of a thermal neutron releases 7.9 MeV energy through the emission of competing conversion electrons, Auger electrons, characteristic K X-rays, and gamma rays. Depending on the energy level (K, L, M, or *N* shell) of the conversion electron, the emission electron will be in the energy range of 29–182 keV and only 1% of the energy is transported by the Auger and conversion electrons, which accounts for 79 keV [9–11] (see Table 1).

$$^{0}n_1 + {}^{155}\mathrm{Gd} \rightarrow {}^{156}\mathrm{Gd}^{*} \rightarrow {}^{156}\mathrm{Gd} + \gamma + \text{conversion electron} + \text{X-rays} + \text{Auger electrons}\ ;\ Q = 8.5\ \text{MeV} \quad (1)$$

$$^{0}n_1 + {}^{157}\mathrm{Gd} \rightarrow {}^{158}\mathrm{Gd}^{*} \rightarrow {}^{158}\mathrm{Gd} + \gamma + \text{conversion electrons} + \text{X-rays} + \text{Auger electrons}\ ;\ Q = 7.9\ \text{MeV} \quad (2)$$

The reaction Q-value energies 8.536 and 7.937 MeV, produce a number of high energy γ-decays, typically above 1 MeV, which are not of primary interest in this work due to their low probability of interaction in the typical scintillator layer thickness of < 1 mm. The resulting de-excitations also produce transitions through numerous low-lying states, which are much more likely to be stopped within a relatively small scintillator. The thermal neutron capture cross-sections of ^{155}Gd and ^{157}Gd are sufficiently large that the thermal neutron reaction occurs within tens of micrometers of the scintillator surface. Hence there is a high likelihood of escape by the 43 keV gadolinium K-shell X-ray for approximately half of the internal conversion events. These events produce a low energy peak due to the conversion electrons that only travel a few micrometers in the scintillator.

In this work, Gd_2O_3:Eu^{3+} and $GdBO_3$:Eu^{3+} phosphor materials were successfully synthesized through a simple precipitation process and subsequent firing as scintillators for thermal neutron detection.

2. Experimental

The materials described throughout this section are gadolinium oxide (99.5%, A.M.P.E.R.E. Industrie, France), europium oxide (99.5%, AMR, China), urea, boric acid (99.5%, Fisons Scientific Equipment), HNO_3 (Fisher Scientific) and phosphor medium (7153E, DUPONT).

2.1. Preparation of Gd_2O_3:Eu and $GdBO_3$:Eu phosphors

The standard method, urea homogeneous precipitation [14], was used to prepare spherical precursors of Gd_2O_3:Eu^{3+} phosphors. The $Gd(NO_3)_3$ stock solution (0.25 M) was prepared by dissolving Gd_2O_3 in dilute HNO_3. Similarly, $Eu(NO_3)_3$ stock solution (0.25 M, 2 mol % diluted) was prepared.

To suitable amounts of $Gd(NO_3)_3$ stock solution, suitable amounts of $Eu(NO_3)_3$ stock solution as well as urea were added in a beaker, dissolved, and diluted to 500 mL by deionized water. The concentrations of [Gd^{3+}+ Eu^{3+}] and urea in the final solution were 0.025 and 0.5 M respectively; [Eu^{3+}]/[Gd^{3+}] was 5% mol. The solution was kept boiling on a hot plate until turbidity was observed, then aged for 1 h. The precipitates above were washed using deionized water several times and filtered. The precipitates were then dried at 60 °C in an oven, and soft white powders resulted. To convert these powders to phosphors, they were fired at 980 °C overnight. Fine particles were separated from large particles using an ultrasonic bath and dried at 60 °C in an oven. The powder was ground using agate mortar and pestle.

To investigate the relationship between luminescence and firing temperature the samples were fired at three different temperatures (700 °C, 980 °C, and 1050 °C).

Similarly, $GdBO_3$:Eu phosphor samples were also prepared [15,16].

2.2. Preparation of scintillator layer

Then 0.5 g of Gd_2O_3:Eu^{3+} powder was mixed with a binder (phosphor medium) using a speed mixer (20 s, 3300 rpm). A fine paste of Gd_2O_3:$Eu^{3+}$was formed. Then scintillator layers (thickness ~100 μm) were deposited on a glass substrate by the K-bar technique and dried at 60 °C in an oven. Before deposition, the glass substrate was cleaned with ethanol. Similarly, thin scintillator layers of $GdBO_3$:Eu^{3+} were prepared.

2.3. Characterization of physical properties

The surface morphology of the Gd_2O_3:Eu^{3+} and $GdBO_3$:Eu^{3+} samples was examined by scanning electron microscopy (SEM) and the fluorescence spectra were obtained by laser-induced spectroscopy.

2.4. Testing with neutrons

The samples were irradiated with a Deuterium–Deuterium (D–D) source emitting 2.5 MeV neutrons. To produce thermal neutrons a 15 cm thick HDPE moderator cube was used. The neutrons passed through about 10 cm (between HDPE and detector) of air before reaching the samples. The pulse height distribution from irradiating the Gd_2O_3:Eu^{3+} and $GdBO_3$:Eu^{3+} samples with thermal neutrons was obtained using a custom designed Bridgeport SiPM MCA (model no: SIPM 1K_BC36_H50) using a Broadcom 6 × 6 mm^2 SiPM which has a peak spectral sensitivity around 420 nm.

2.5. Simulation with FLUKA

FLUKA is a Fortran-based Monte Carlo code used to calculate particle transport and interactions with FLAIR as the interface for editing the input file, executing the code, and visualizing the output files [17–19]. The simulation activity in this study was done using the FLUKA version 4.2.0 and FLAIR 3.1–15 version installed in Centos (Linux-based operating system). FLUKA offers numerous different estimators that can be used to score various quantities of interest. The DETECT card was used for acquiring the energy deposition spectrum. The light produced in scintillator material is emitted in all directions. Only a limited fraction of it reaches the surface where SiPM is mounted. Thus the USRBDX card is used to calculate the light that passes through the boundary. All these functions (cards) are used for finding the response function of the scintillator. As well as visualization of neutron fluence, corresponding energy deposition, light photons produced, and light passes through the boundary were carried out for each scintillator type. To obtain a reasonable statistical error (<2%), 10^8 particles were run with five cycles.

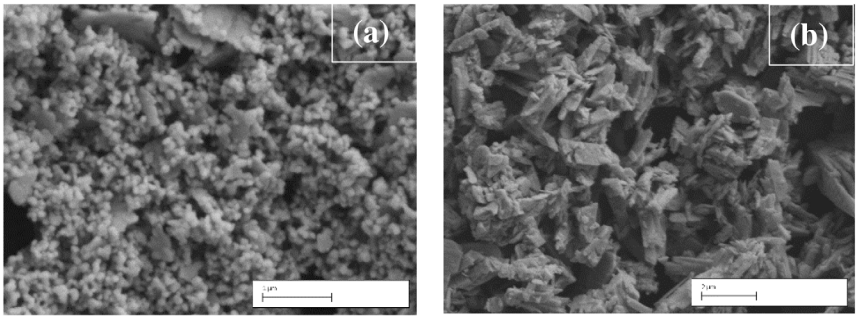

Fig. 1. SEM image of (a) $Gd_2O_3:Eu^{3+}$ and (b) $GdBO_3:Eu^{3+}$.

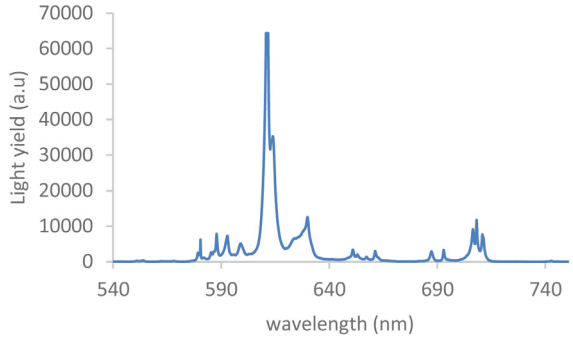

Fig. 2. Fluorescence spectra of $Gd_2O_3:Eu^{3+}$ (fired at 980 °C).

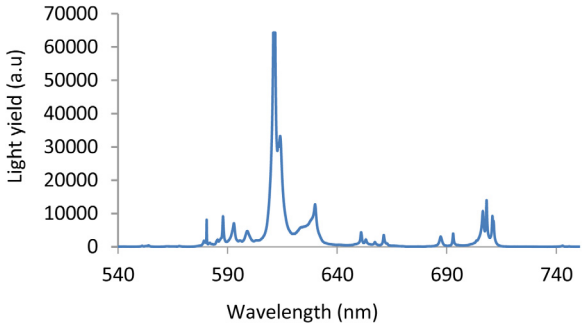

Fig. 3. Fluorescence spectra of $GdBO_3:Eu^{3+}$ (fired at 800 °C).

3. Results and discussions

3.1. Characterization of samples

Fig. 1(a) presents an SEM micrograph of the $Gd_2O_3:Eu^{3+}$ sample. Fig. 1(b) shows an SEM micrograph of the $GdBO_3:Eu^{3+}$ sample.

The $Gd_2O_3:Eu^{3+}$ precursors prepared by the standard method have an approximately spherical shape with a diameter of about 0.1 μm. $GdBO_3:Eu^{3+}$ precursors have a rod shape of 0.5-2 μm in size. Crystallinity can be observed in both materials.

Figs. 2 and 3 shows fluorescence spectra of $Gd_2O_3:Eu^{3+}$ and $GdBO_3:Eu^{3+}$ samples recorded from 540–750 nm by using laser-induced spectroscopy. Under the excitation of the laser (532 nm), $Gd_2O_3:Eu^{3+}$ and $GdBO_3:Eu^{3+}$ displays the characteristic red emission due to Eu^{3+}.

The charged particles emitting from the reactions (1) and (2) mentioned above consequently excite Eu^{3+} ions and result in the characteristic Eu^{3+} emission peaking around 612 nm that corresponds to the transition of electrons from 5d → 7f energy levels. Spectra consist of 5 sets of lines at 580 nm, 587–600 nm, 611–630 nm, 651–661 nm, and 687–710 nm which are connected to the intra-configurational $^5d_0 \rightarrow {}^7f_0$, $^5d_0 \rightarrow {}^7f_1$, $^5d_0 \rightarrow {}^7f_2$, $^5d_0 \rightarrow {}^7f_3$ and $^5d_0 \rightarrow {}^7f_4$ transitions of Eu^{3+}, respectively. The strongest emission was observed for $^5d_0 \rightarrow {}^7f_2$ transition, followed by $^5d_0 \rightarrow {}^7f_4$ transition.

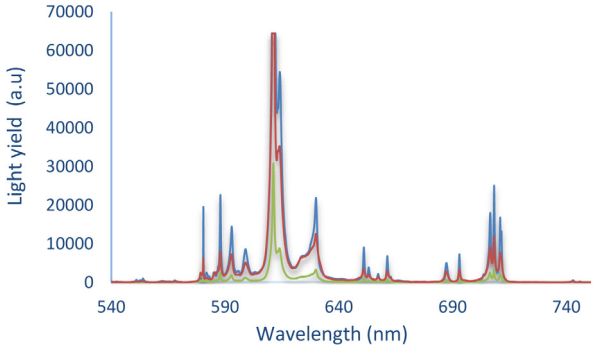

Fig. 4. Fluorescence spectra of $Gd_2O_3:Eu^{3+}$ samples fired at 700 (green), 980 (red), and 1050 °C (blue) (laser applied with 1% filter).

Another primary factor to develop an efficient scintillator is to optimize the light emission properties. In order to study the variation of light emission for different firing temperatures, samples were fired at 700, 980, and 1050 °C.

Fig. 4 shows fluorescence spectra of three $Gd_2O_3:Eu^{3+}$ samples fired at different temperatures recorded from 540–750 nm by using laser-induced spectroscopy. The maximum photoluminescence intensity was observed at 1050 °C firing temperature because higher temperature yields better crystallization.

3.2. Simulated spectrum

As shown in reaction (1) and (2), after the Gd neutron capture event, excited states of the resultant $^{156}Gd^*$ and $^{158}Gd^*$ nuclei are relatively low lying-in energy. In excited states, due to relatively high atomic number of gadolinium ($Z = 64$), this leads to internal conversion electron emission leaving vacancies in the atomic shells, orbital electron shuffling occurs leading to the emission of characteristic X-rays, which is a competing process to gamma-ray emission. Therefore, neutron capture process of natural gadolinium produces characteristic X-rays as well as prompt gamma rays.

The simulated spectrum from FLUKA for $Gd_2O_3:Eu^{3+}$ and $GdBO_3:Eu^{3+}$ shows in Fig. 5. Atoms in excited states de-excite by emitting X-rays mainly between 40–50 keV for the K-shell and 6–7 keV for the L-shell and low energy Auger electrons. The combined 1st excited state to ground state transitions for ^{156}Gd and ^{158}Gd being at ~82 keV.

3.3. Neutron irradiation

As explained in the previous section, the fabricated Gd-based scintillator should produce a pulse height spectrum with features that are

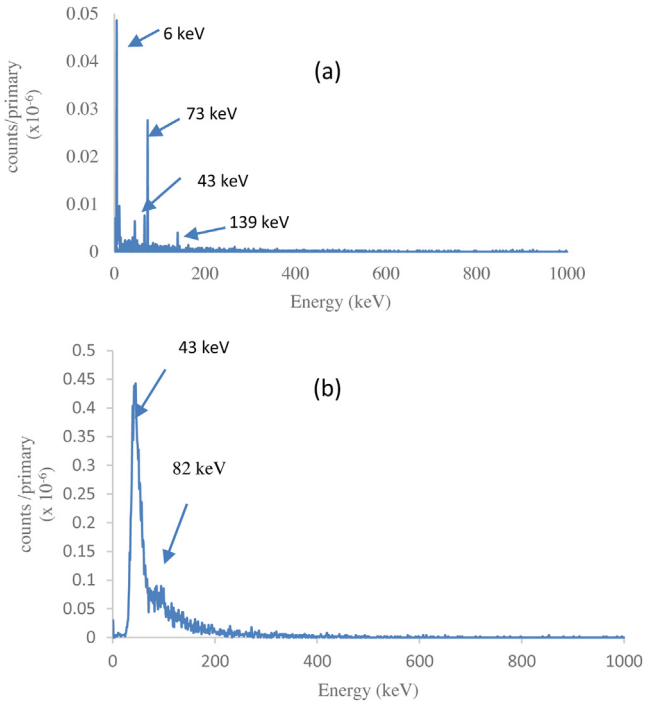

Fig. 5. Simulated pulse height spectrum of (a) $Gd_2O_3:Eu^{3+}$ (b) $GdBO_3:Eu^{3+}$.

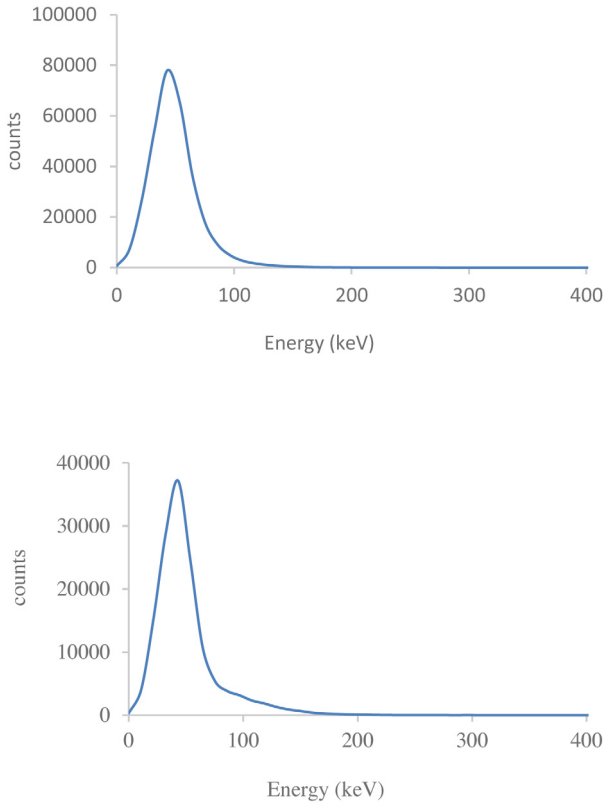

Fig. 6. (a) Pulse height spectrum of $Gd_2O_3:Eu^{3+}$(fired at 980 °C) (b) Pulse height spectrum of $GdBO_3:Eu^{3+}$ (fired at 800 °C).

attributable to characteristics X-rays and prompt gamma rays following a neutron capture.

As seen in the experimental spectrum, only a convolution of the low energy peaks ~43 keV are visible (Figs. 6, and 7), the intrinsic noise

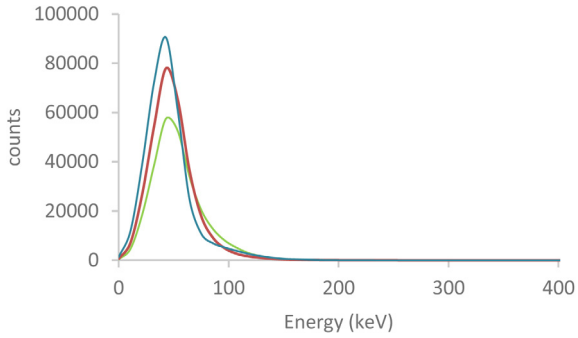

Fig. 7. Pulse height spectra of $Gd_2O_3:Eu^{3+}$ samples fired at 700 (green), 980 (red), and 1050 °C (blue).

of the detector system is negligible compared to the broad peak shown in these pulse height spectra.

There are two sources of gamma rays that are concerned when gadolinium is used as a neutron capture element, one is external gamma ray accompanying neutron field and the other is neutron-activated internal prompt gamma rays. The thermal neutron capture cross-sections of ^{155}Gd and ^{157}Gd are sufficiently large that the thermal neutron reaction occurs within tens of micrometers of the surface of the detector. Hence there is a high likelihood of escape by the 43 keV gadolinium K-shell X-ray for approximately half of the internal conversion events. These events produce a low energy peak due to the conversion electrons that only travel a few micrometers in the scintillator. The size of the prepared scintillator is small (1 cm ^{2} and 100 μm thickness). Such thin film devices are likely to be gamma blind, because of the long attenuation length of gamma radiation, at energies of 200 keV and above where for 0.1 mm thickness layers, the photoelectron interaction probability is calculated to be < 2%) compared to the interaction probability for thermal and epithermal neutrons. However there is the distinct possibility that X-rays, caused by inelastic scatting processes in materials placed between the source and the detector, may cause K-shell Auger electron emission.

Consequently, there is a range of thicknesses where the Gd-doped film is opaque to neutrons and somewhat transparent to typical gamma rays. For the devices we have measured, the high energy gammas have a mean free path much greater than the active region and can be ignored, not only based on cross-section but because the experimental pulse height spectra are the characteristic of the expected electron energy spectrum.

Fig. 7 shows that the peak response of the $Gd_2O_3:Eu^{3+}$ scintillator layers are increasing when the firing temperature is increased.

This clarifies that, for samples fired at 700–1050 °C, the luminescence increased because higher temperature firing yields better crystallization, thus increasing the detection efficiency of the samples. Therefore, emission from these gadolinium based scintillators improves through better crystallization.

4. Conclusion

The scintillation properties of $Gd_2O_3:Eu^{3+}$ and $GdBO_3:Eu^{3+}$ have been investigated in this work. The $Gd_2O_3:Eu^{3+}$ and $GdBO_3:Eu^{3+}$ were tested as scintillators for thermal neutron detection. In addition, the photoluminescence properties for different firing temperatures were also investigated. These results show that the detection of K X-ray emission from gadolinium oxide based scintillators improves significantly through better crystallization at higher temperatures.

Declaration of competing interest

The authors declare that they have no known competing financial interests or personal relationships that could have appeared to influence the work reported in this paper.

Data availability

Supplementary data to this article can be found online at DOI: http://10.6084/m9.figshare.20521023

Acknowledgments

This work was performed as a part of a Ph.D. project funded under EPSRC, United Kingdom DTP grant EP/T518116/1. The authors would like to thank EPSRC for financial support, Brunel University London, United Kingdom for facilitating this research, and STFC at the Rutherford Appleton Laboratory for providing access to the NILE neutron beamline for this research.

References

[1] E.V. Ryabeva, V.V. Kadilin, V.A. Idalov, Use of neutron scintillation detectors as a substitute for helium-3 counters in radiation monitors, At. Energy 127 (2019) 51–55.
[2] R.T. Kouzes, K.E. Conlin, J.H. Ely, L.E. Erikson, W.J. Kernan, A.T. Lintereur, E.R. Siciliano, D.L. Stephens, D.C. Stromswold, R.M. Van Ginhoven, M.L. Woodring, Alternatives to 3He for neutron detection for homeland security, Nucl. Instrum. Methods Phys. Res. A 623 (2010) 1035–1045.
[3] D.A. Shea, D. Morgan, The Helium-3 Shortage: Supply, Demand, and Options for Congress, CRS Report for Congress, 2010, www.crs.gov. (last accessed on 01 2022).
[4] V. Fernandez, Rare-earth elements market: A historical and financial perspective, Resour. Policy 53 (2017) 26–45.
[5] ANSI, N42.35-2006 (2006) https://webstore.ansi.org/.
[6] ANSI, N42.34-2006 (2006) https://webstore.ansi.org/.
[7] IEC 62244, Radiation protection instrumentation-installed radiation monitors for the detection of radioactive and special nuclear materials at national borders, 2006, https://www.iec.ch/homepage.
[8] J.L. Grafe, F.E. McNeill, D.R. Chettle, S.H. Byun, Characteristic X-ray emission in gadolinium following neutron capture as an improved method of in vivo measurements: A comparison between feasibility experiment and Monte Carlo simulation, Nucl. Instrum. Methods Phys. Res. B 281 (2012) 21–25.
[9] P. Perani, A. Tomanin, S. Pozzi, J. Dolan, E. Miller, M. Flaska, M. Bagttaglieri, R. De Vita, L. Ficini, G. Ottonello, G. Ricco, G. Dermody, C. Glies, Testing on novel neutron detectors as an alternative to ^{3}He for security applications, Nucl. Instrum. Methods Phys. Res. A 696 (2012) 110–120.
[10] C.W.E. van Eijk, Inorganic scintillators for thermal neutron detection, Radiat. Meas. 38 (2004) 337–342.
[11] P. Kandlakunta, L. Lao, Gamma-ray rejection or detection with gadolinium as a converter, Radiat. Prot. Dosim. 151 (2012) 586–590.
[12] K.W. Van Delinder, R. Khan, J.L. Gräfe, Neutron activation of gadolinium for ion therapy: a Monte Carlo study of charged particle beams, Sci. Rep. 10 (2020) 13417.
[13] D. Schultz, B. Blasy, J.C. Santana, C. Young, J.C. Petrosky, J.W. McClory, D. LaGraffe, J.I. Brand, J. Tang, W. Wang, N. Schemm, S. Balkir, M. Bauer, I. Ketsman, R.W. Fairchild, Y.B. Losovyj, P.A. Dowben, The K-shell auger electron spectrum of gadolinium obtained using neutron capture in a solid-state device, J. Phys. D: Appl. Phys. 43 (2010) 075502.
[14] X. Jing, T. Ireland, C. Gibbons, D.J. Barber, J. Silver, A. Vecht, G. Fern, P. Trowga, D.C. Morton, Control of Y2O3:Eu spherical particle phosphor size, assembly properties, and performance for FED and HDTV, J. Electrochem. Soc. 146 (1999) 4654–4658.
[15] K. Aiste, G. Raimondas, J. Remigius, E. David, J. Thomas, K. Arturas, Luminescence and luminescence quenching of efficient $GdBO_5O_5:Eu^{3+}$ red phosphors, J. Lumin. 192 (2017) 520–526.
[16] C. Ahdida, D. Bozzato, D. Calzolari, F. Cerutti, N. Charitonidis, A. Cimmino, A. Coronetti, G.L. D'Alessandro, A. Donadon Servelle, L.S. Esposito, R. Froeschl, R. García Alía, A. Gerbershagen, S. Gilardoni, D. Horváth, G. Hugo, A. Infantino, V. Kouskoura, A. Lechner, B. Lefebvre, G. Lerner, M. Magistris, A. Manousos, G. Moryc, F. Ogallar Ruiz, F. Pozzi, D. Prelipcean, S. Roesler, R. Rossi, M. Sabaté Gilarte, F. Salvat Pujol, P. Schoofs, V. Stránský, C. Theis, A. Tsinganis, R. Versaci, V. Vlachoudis, A. Waets, M. Widorski, New capabilities of the FLUKA multi-purpose code, Front. Phys. 9 (2022) 788253.
[17] G. Battistoni, T. Boehlen, F. Cerutti, P.W. Chin, L.S. Esposito, A. Fassò, A. Ferrari, A. Lechner, A. Empl, A. Mairani, A. Mereghetti, P. Garcia Ortega, J. Ranft, S. Roesler, P.R. Sala, V. Vlachoudis, G. Smirnov, Overview of the FLUKA code, Ann. Nucl. Energy 82 (2015) 10–18.
[18] V. Vlachoudis, FLAIR: A powerful but user-friendly graphical interface for FLUKA, in: Proc. Int. Conf. on Mathematics, Computational Methods & Reactor Physics, M & C 2009, Saratoga Springs, New York, 2009.
[19] https://fluka.cern/ (last accessed on 01.08.2022).